First International Symposium on Marine Propulsors
smp'09, Trondheim, Norway, June 2009

Simulation of Viscous Flow around a Ducted Propeller with Rudder Using Different RANS-Based Approaches

A. Sánchez-Caja[1], Tuomas P. Sipilä[1] and J.V. Pylkkänen[2]

[1,2]VTT Technical Research Center of Finland, [2]ret.

ABSTRACT

Within EU Project SUPERPROP, the flow around a ducted propeller located in front of a rudder has been numerically simulated and analyzed using different RANS approaches. The presence of the rudder makes the velocities at the propeller plane non-symmetric, which results in a flow of unsteady nature. Unsteady flows can sometimes be approximated using simplifications which reduce the hydrodynamic problem to a steady-state one, whilst the prediction accuracy remains reasonable. The main two simplifications are the mixing plane approach and the quasi-steady approach. This paper compares calculations made with these two approaches to time-accurate computations. The computations are performed on a ducted propeller unit of a fishing vessel subject to investigation within EU project SUPERPROP. Comparison of thrusting forces obtained with the different approaches is presented for the various components of the propulsion unit. Details of the flow at particular zones illustrate the character of the simplifications for this particular configuration. RANS code FINFLO was used in the calculations.

Keywords

RANS, unsteady, quasi-steady, mixing plane, ducted propeller.

1 INTRODUCTION

Flow unsteadiness in a duct- propeller- rudder configuration is caused mainly by the following phenomena: (a) viscous interaction of the rotating blades with the viscous wake and detached vortices generated by ship hull, (b) potential (pressure-based) interaction due to relative motion of the blades with respect to the rudder and hull, (c) viscous interaction due to shedding of vortices from the propeller blades and hub impinging on the rudder.

Even in the case where the propulsion unit is studied in a simplified axisymmetric onset flow, the presence of the rudder induces flow unsteadiness by introducing asymmetry into the problem. In particular the rudder affects the flow at the propeller plane by decreasing the magnitude of the velocity field, in other words by producing a flow blockage to the propeller. The closer the rudder is to the propeller, the larger the blockage will be. Usually the flow retardation due to the presence of the rudder is smaller than the flow acceleration induced by the duct in flow accelerating nozzles. Behind the duct, the presence of the rudder alters strongly the otherwise almost axisymmetric pattern of the flow contraction by increasing the contraction on the suction side of the rudder and reducing it on the pressure side.

Typically, unsteady RANS calculations for ducted propellers are made by placing within the computational mesh a set of stationary blocks surrounding the duct and rudder, and a set of rotating blocks around the propeller blades. Simplifications may be introduced in the computational method in order to reduce the long CPU times involved in the time-accurate computations. At the same time the exact propeller geometry can be preserved within the numerical approach. The quasi-steady and the mixing plane methods are possible approximate solutions that meet such requirements.

For these approximate solutions the flow is reduced to a steady-state regime with rotating blocks that *do not rotate* during the computation. Special boundary conditions may be enforced at the interface between rotating and stationary blocks depending on the nature of the approach followed. However, not all unsteady propeller flows can be reasonably modeled using methods based on steady - state simplifications. As stated by Li et al (2005) the method is not appropriate for cases where the flow enters and leaves the outer boundary of a rotating domain like in propellers under inclined onset flows. Moreover, for axial flows a badly chosen location of the interface between the rotating and stationary blocks may introduce non-physical numerical blockage (Sánchez-Caja et al, 2008).

In the present paper a comparison of the 'exact' time-accurate RANS solution to the simplified quasi-steady and mixing plane ones is presented for a propulsion unit consisting of a propeller, duct and rudder, studied in EU project SUPERPROP. In order to minimize errors involved in the simplified approaches, the location of the interface between rotating and stationary blocks was studied in a previous work (Sánchez-Caja et al, 2008). The present paper shows that in cases like propeller-duct-rudder configurations under axisymmetric axial onset

flow, RANS methods based on steady-state simplifications may yield reasonable results and consequently speed up the propeller analysis or design process.

2 NUMERICAL METHODS

The flow simulation in FINFLO is based on the solution of the RANS equations by the pseudo-compressibility method. FINFLO solves the RANS equations by a finite volume method. The solution is extended to the wall and is based on approximately factorized time-integration with local time-stepping. The code uses either Roe's flux-difference splitting or Van Leer's flux-vector splitting for compressible flows and an upwind-based scheme for incompressible flows. In the latter case, the pressure is center-differenced and a damping term is added via a convective velocity. A multigrid method is used for the acceleration of convergence. Solutions in coarse grid levels are used as starting point for the calculation in order to accelerate convergence.

For the time-accurate computations the interface between the rotating propeller grid blocks and the surrounding stationary blocks is treated using a sliding-mesh technique, where the grid lines across the block interface are discontinuous. The solution for a block is interpolated using the solution in the neighboring block. A mass conserving interpolation is made between the connecting blocks at every time step. A detailed description of the numerical method including discretization of the governing equations, solution algorithm, etc. can be found in Sanchez-Caja et al. (1999 and 2000). Chien's k-epsilon turbulence model was used in the calculation.

Unsteady flows can be approximated using mixing plane and quasi-steady methods. In the mixing-plane approach the flow quantities for both the rotating and non-rotating blocks are circumferentially averaged on both sides of the common interface and then transferred to the ghost cells as boundary values. In the quasi-steady approach the rotating and non-rotating blocks are connected without any averaging process.

The simplified approaches may give sensible results when the interaction between the rotating and stationary domains is weak. For axial flows even though the velocities everywhere are expressed in inertial coordinates, the flow disturbances are convected using different reference frames on the blocks at each side of the interface. The transition of the flow at the interface should be smooth without interferences of solid boundaries located nearby. This is especially critical for solid boundaries located downstream of the interface blocking the flow.

3 GEOMETRY AND MESH

The propeller used in the simulation was a four-bladed one with 2.6 m diameter and about 0.96 pitch diameter ratio. The computations were made at a model scale ratio of 1:12. The duct length ratio was L/D=0.5 and the rudder length was two duct lengths.

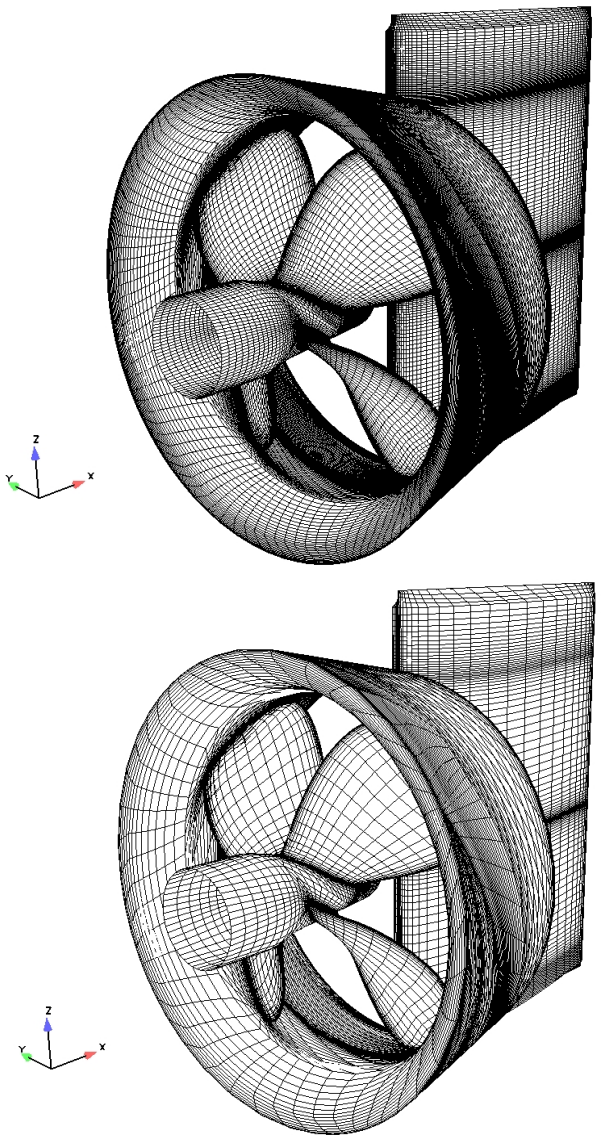

Figure 1. Surfaces of the propeller, duct and rudder, fine (above) and medium-size (below) meshes. Front view.

The computational mesh was structured and continuous. C-topology was selected around the propeller blades, which allowed having cells concentrated on the propeller wake. O-topology was used around the duct and O-H around the rudder.

A fine and a medium-size grid were built and consisted of 9.5 and 1.2 million cells respectively, distributed in 23 blocks. The medium size mesh was obtained by removing every other grid line from the finer mesh, which makes y^+ vary by a factor of about 2 between the meshes. Figure 1 shows the discretization used on the solid surfaces for the fine and the medium size mesh.

Figures 2 and 3 show a grid detail behind the propeller hub. A singularity in the grid topology at the propeller axis was avoided by using a modified butterfly topology where the central block was removed and reduced to a connectivity surface. The removal of the central block makes the mesh smaller compared to a mesh based on the traditional butterfly topology.

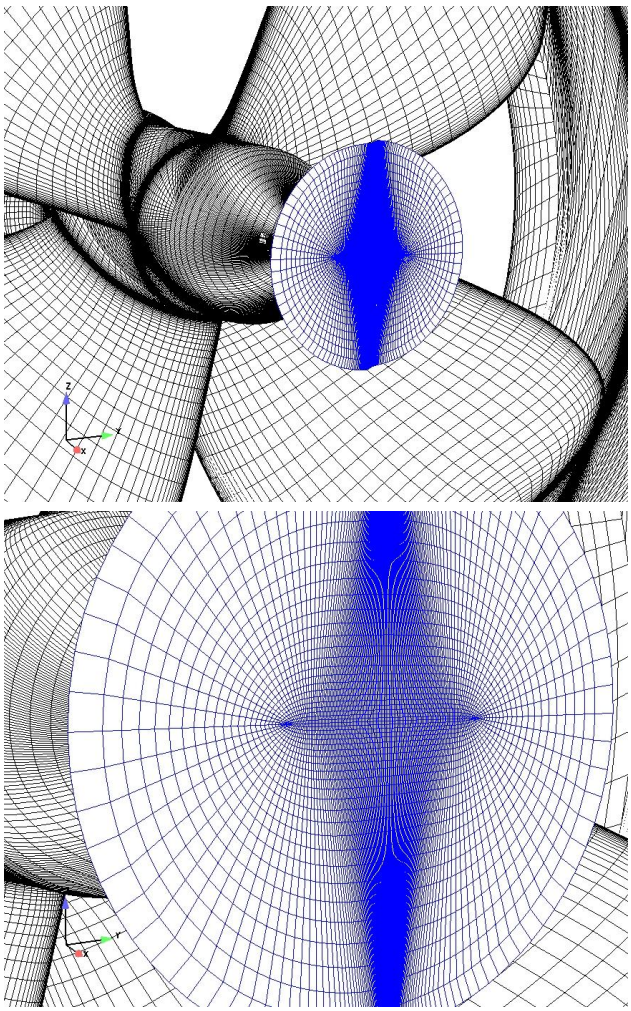

Figure 2. Detail of grid construction behind the propeller hub at the axis of rotation. Modified butterfly topology. Back view.

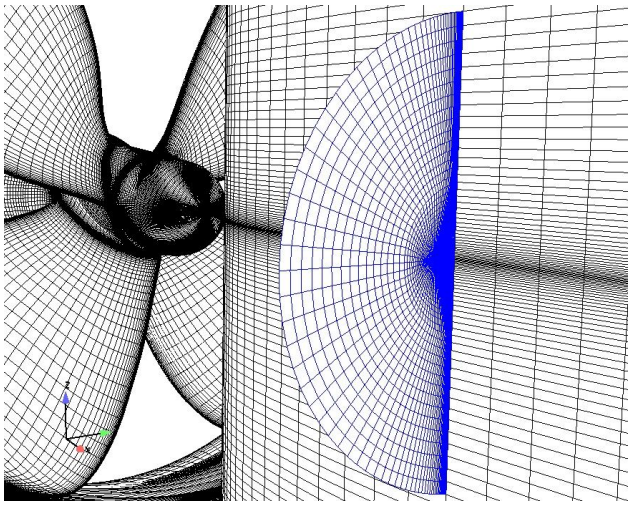

Figure 3. Detail of grid construction on the rudder. Back view.

The sliding surface located between the propeller and the rudder has 288 cells in the circumferential direction for the fine grid. Figure 3 illustrates the topology used over the rudder surface. The time accurate calculations were made on the medium-size grid in order to decrease the CPU time. For homogeneous treatment of the results the same mesh was used in all computations.

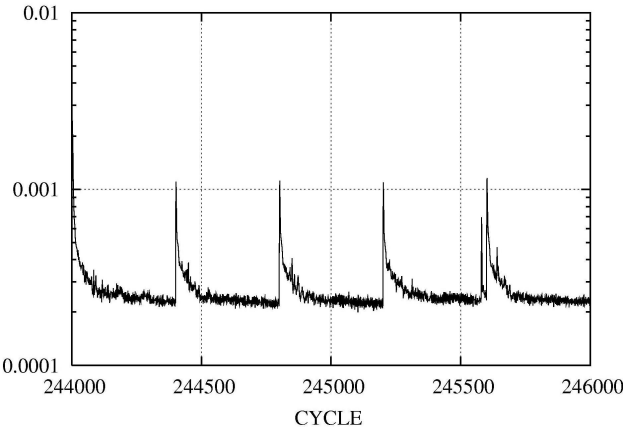

Figure 4. Convergence history of x-momentum residuals. Time-accurate computation.

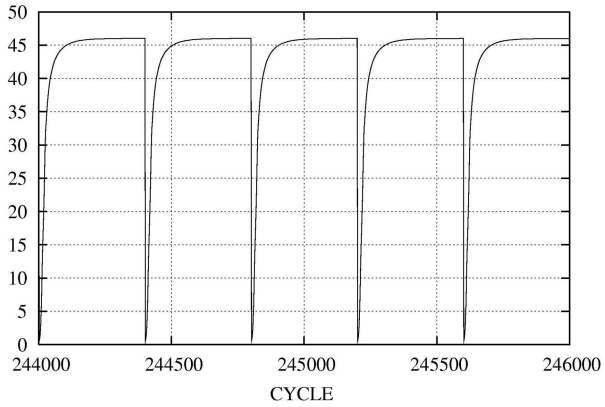

Figure 5. Convergence history of turbulent kinetic energy. Time-accurate computation.

4 INITIAL AND BOUNDARY CONDITIONS

The inflow to the ducted propeller unit was assumed uniform and the advance number for the ducted propeller was J=0.526. The boundary conditions were as follows. The downstream cap of the hub and surfaces of the propeller blades are rotating solid walls with boundary conditions enforcing the velocity field to match the propeller rotational speed. The duct and rudder surfaces are non-rotating solid walls. At the computational infinity the boundary conditions consist of uniform flow applied to the inlet and peripheral surfaces, and zero streamwise gradients of the flow variables as well as zero pressure difference at the outlet.

The sliding surfaces used in the time accurate computations were located with enough axial separation from solid boundaries of the neighboring blocks. This was made in order to avoid using a different mesh in the quasi-steady and mixing-plane calculation. These latter approaches require such treatment in order to avoid

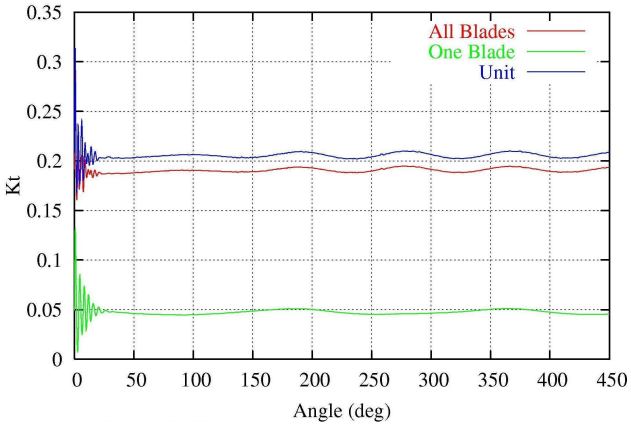

Figure 6. Convergence history of thrust for a single blade (lower curve), for all blades (middle curve) and for the entire propulsion unit (upper curve). Time-accurate computation. J=0.526.

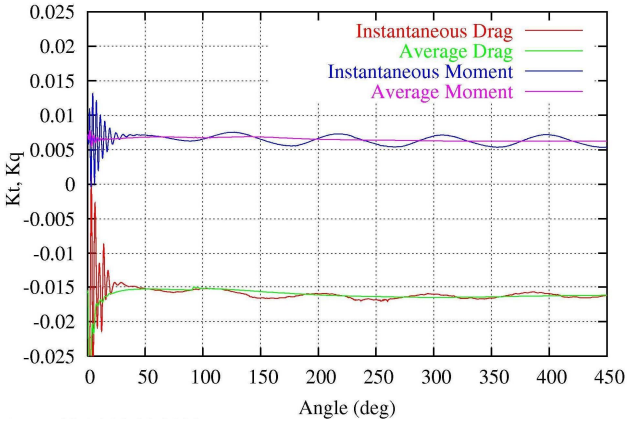

Figure 7. Convergence history of drag (lower curve) and OX momentum forces (upper curve) on the rudder. Time-accurate computation. J=0.526.

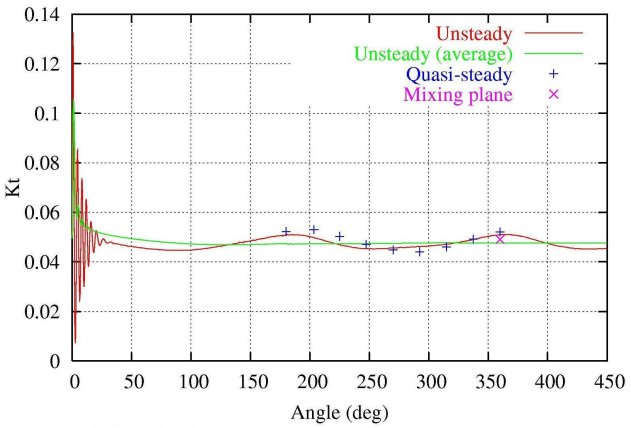

Figure 8. Comparison of thrust on a single blade predicted by the time-accurate, quasi-steady and the mixing plane approaches. J=0.526.

strong interaction between the rotating and stationary domains. For this particular study two sliding surfaces were used, one located midway between the downstream edge of the hub and the blade trailing edge, and the other just in front of the duct. These distances seem sufficient to avoid strong non-physical domain interaction.

5 CONVERGENCE AND ANALYSIS OF FORCES

The time-accurate computations were performed on Xeon™ with 8 3.0 GHz processors. Time steps of half degree were employed. The computation lasted about one week.

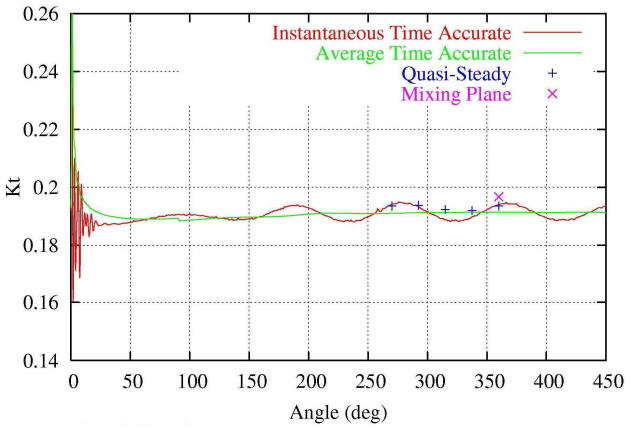

Figure 9. Comparison of thrust on all blades predicted by the time-accurate, quasi-steady and the mixing plane approaches. J=0.526.

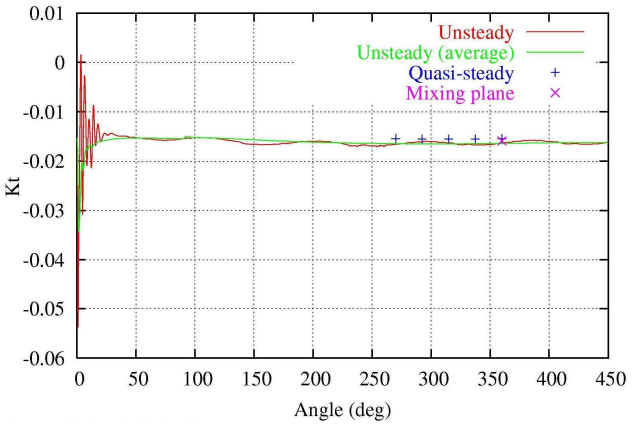

Figure 10. Comparison of drag on the rudder predicted by the time-accurate, quasi-steady and the mixing plane approaches. J=0.526.

Figure 4 shows the convergence history of residuals for the x-velocity momentum in the 2nd grid level (medium-size mesh) and Figure 5 the convergence of turbulent kinetic energy. Figure 6 shows the convergence history of blade thrust for one and all blades together with that of the overall unit thrust (including duct thrust and rudder drag). The flow is periodic with the blade passing frequency, which in this case corresponds to an angular variation of 90 deg. The presence of the rudder makes the forces on each single blade 180-deg periodic. Figure 7 shows the convergence of drag (negative thrust) and OX momentum for the forces on the rudder. The amplitude of

fluctuations in rudder drag is smaller than those in blade thrust. The values of the unsteady calculations in the Figures are averaged over an angular interval of 90 deg. The upper limit of the interval coincides with the curve point represented in the Figures.

Four propeller positions corresponding to blade angle increments of 22.5 deg were analyzed with the quasi-steady approach on the medium-size mesh. The computations were conducted until the turbulent kinetic energy reached a constant value using exactly same computational conditions (same Courant numbers, multigrid levels, number of iterations, etc.) on each of the four propeller positions. More information on quasi-steady computations made on the fine grid and a study on computational interaction between stationary and rotating domains was presented in Sánchez-Caja et al (2008).

Figure 8 compares the thrust on a single blade, obtained using the unsteady, quasi-steady and the mixing plane approaches. Figure 9 shows the comparison for all blades. The amplitude of force fluctuation for the single blade is similar in the quasi-steady and in the unsteady computations, being the former more sinusoidal, in other words more symmetric. This results in a stronger cancelation of force fluctuation for the forces on all the blades in the quasi-steady approach relative to the unsteady one. The noticeable fluctuations observed in the overall forces on the blades in the unsteady case results not only from the lack of symmetry in the single-blade unsteady thrust but also from the fact that blades separated 180 degrees produce forces in the same phase. Stronger cancelation of overall blade forces would have been obtained for a propeller with an odd number of blades.

In Figure 8 the location of force maxima and minima are somewhat shifted in the quasi-steady computation relative to the unsteady one. The explanation must be found in the different way that the approaches treat the convection of flow disturbances downstream in the stationary blocks. The average values of quasi-steady and mixing-plane blade thrust are slightly larger than those obtained with the unsteady approach.

Figure 10 compares the drag on the rudder obtained using the unsteady, quasi-steady and the mixing plane approaches. The drag is somewhat larger in the unsteady computation than in the computations of the simplified approaches. However, the differences amount to less than half percent of total unit thrust (see Table I).

Table I compares computational forces (in percentages) obtained following the three approaches for the ducted propeller with rudder working at J=0.526. The time-accurate and quasi-steady results are averaged to facilitate the comparison between the approaches. The values of thrust (or torque) are made non-dimensional with the total thrust (or torque) obtained from the time-accurate computation. The differences between the quasi-steady and the time-accurate results are less than one percent. The maximum differences between the mixing plane and the time-accurate results are 3 percent.

Table I. Average thrust force and torque calculated with different RANS approaches in percentages of total time-accurate thrust (or torque) at J=0.526. Medium-size grid.

	Time-accurate	Mixing plane	Quasi-steady
$K_{T\ all\ blades}$	92.8	95.5	93.5
$K_{T\ duct}$	16.1	16.5	16.0
$K_{T\ rudder}$	-7.9	-7.8	-7.5
$K_{T\ total}$	100.0	103.1	100.8
$K_{Q\ blade}$	100.0	102.9	100.16

Table II compares computational efficiencies (in percentages) obtained following the three approaches for the same case. The time-accurate and quasi-steady instantaneous efficiencies are averaged to facilitate the comparison to the mixing plane approach. The values of efficiency are relative to the total unit efficiency obtained from the time-accurate computation. Now the mixing plane approach rather than the quasi-steady one yields results closer to the time-accurate efficiencies. The largest differences between the approaches are about half of a percent.

Table II. Average efficiency calculated with different RANS approaches for the ducted propeller at J=0.526 in percentages of unit time-accurate efficiency. Medium-size grid.

	Time-accurate	Mixing plane	Quasi-steady
$\eta_{\ blades}$	92.8	92.8	93.3
$\eta_{\ duct+blades}$	108.9	108.9	109.3
$\eta_{\ total}$	100.0	100.2	100.6

6 FLOW ANALYSIS

The differences in flow patterns obtained using the three approaches are illustrated in Figures 11, 12 and 13. They show the convection of the blade wake in a back view (from the rudder) on a cylinder located at r/R=0.65. The Figures correspond to the time-accurate, mixing plane and quasi-steady approach, respectively. In Figures 11, 12 and 13 the blade wake is visualized by contours showing the direction of the flow particles. The contours indicate the angle between the axial and tangential velocity components in the inertial frame of reference. The blade wake appears as the zone of largest angles (above 14 deg).

Figure 11 shows the wake extending far behind the blade for the time-accurate case. The wake is visible as the

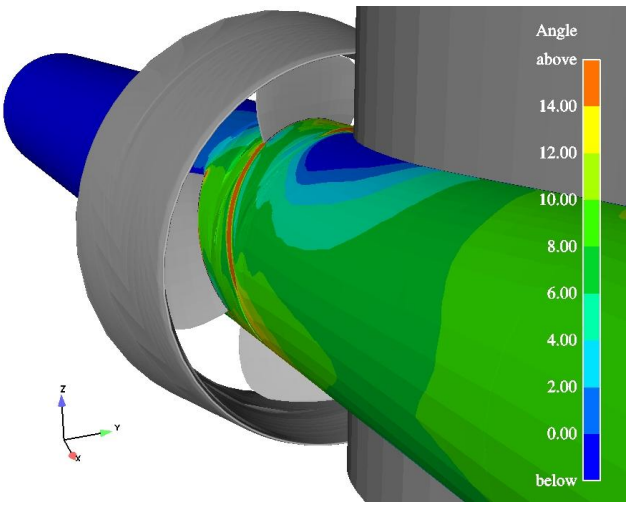

Figure 11. Angle of flow particles located on a cylinder at r/R=0.65. The wake behind the blade is visible as the zone of highest angles. *Time-accurate* computation. Back view.

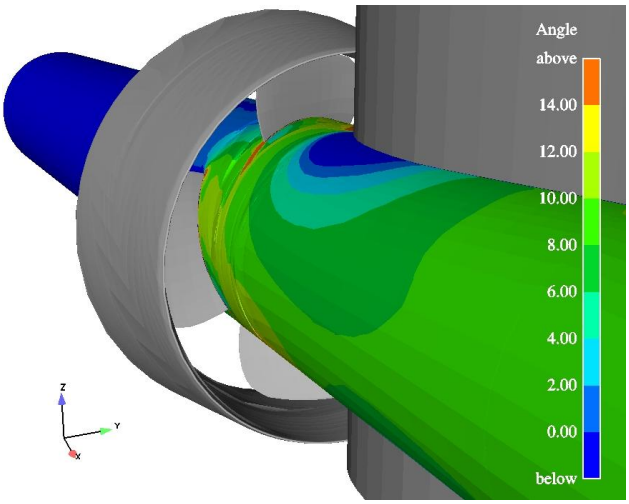

Figure 12. Angle of flow particles located on a cylinder at r/R=0.65. *Mixing plane* computation. Back view.

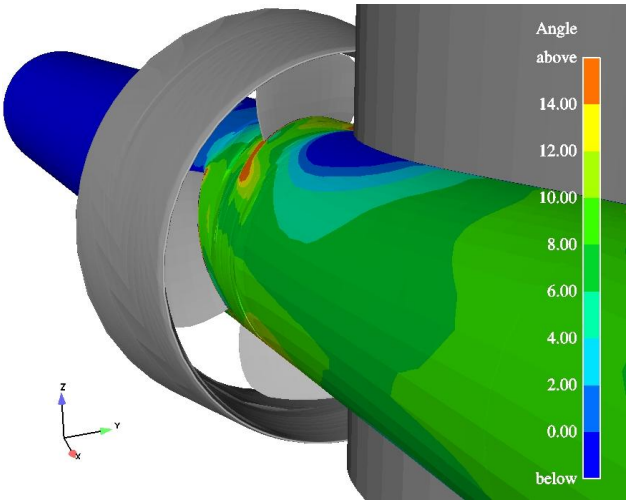

Figure 13. Angle of flow particles located on a cylinder at r/R=0.65. The wake behind the blade is visible as the zone of highest angles. *Quasi-steady* computation. Back view.

zone of largest angles. Figure 12 shows that the blade wake suddenly disappears at a short distance behind the blade trailing edge, which coincides with the location of the mixing plane. Figure 13 shows that the blade wake changes direction at the location where the mixing plane was positioned in Fig 12 and then disappears after a short distance due to its interference with the velocity field of the rudder. That location coincides with the interface between the moving and stationary blocks for this quasi-steady computation.

Figures 14 and 15 display the pressure contours obtained at two extreme locations of the blade force fluctuation by the time-accurate and quasi-steady approach, respectively. The ducted propeller is shown from a back view with the rudder removed to facilitate the visualization. They display the blade pressure side. The angles in the Figure captions are referred to the 12 o'clock position. Figure 16 shows the corresponding contours for the mixing plane approach. The qualitative agreement between the approaches is good. Slightly larger pressures are shown for the mixing plane approach, which is in line with the larger values of thrust presented in Table I.

Figure 17 displays the pressure contours obtained by the quasi-steady approach, but in this case the interface between the rotating and stationary blocks is located behind the rudder trailing edge, i.e. downstream too close to the solid boundaries of the rudder, and consequently a numerical blockage appears in the computation. The blockage is apparent in terms of larger pressures at the 12 and 6 o'clock blades, which are located just in front of the rudder.

Figures 18 and 19 display the pressure contours obtained on the rudder by the time-accurate and quasi-steady approach, respectively. The pictures are taken at blade angles of 0 and 45 deg for which the largest differences are found in the pressure patterns.

7 DISCUSSION AND CONCLUSIONS

Unsteady propeller flows can be sometimes approximated using simplified RANS approaches that reduce the hydrodynamic problem to a steady-state one, namely the quasi-steady and the mixing plane approach. The success of the approximations will depend on what are the goals pursued by the propeller designer in a particular case and on the ability of the simplified approaches not to distort such design goals.

For the ducted propeller with rudder considered in this paper the simplified approaches yielded relative to the time-accurate one good prediction of average thrusting forces on the different component of the propulsion unit. The quasi-steady approach was somewhat better in predicting forces, the differences being less than one percent. The mixing plane was better in predicting efficiencies, the differences being less than half percent.

For the successful application of the simplified approaches it is important to maintain the interaction

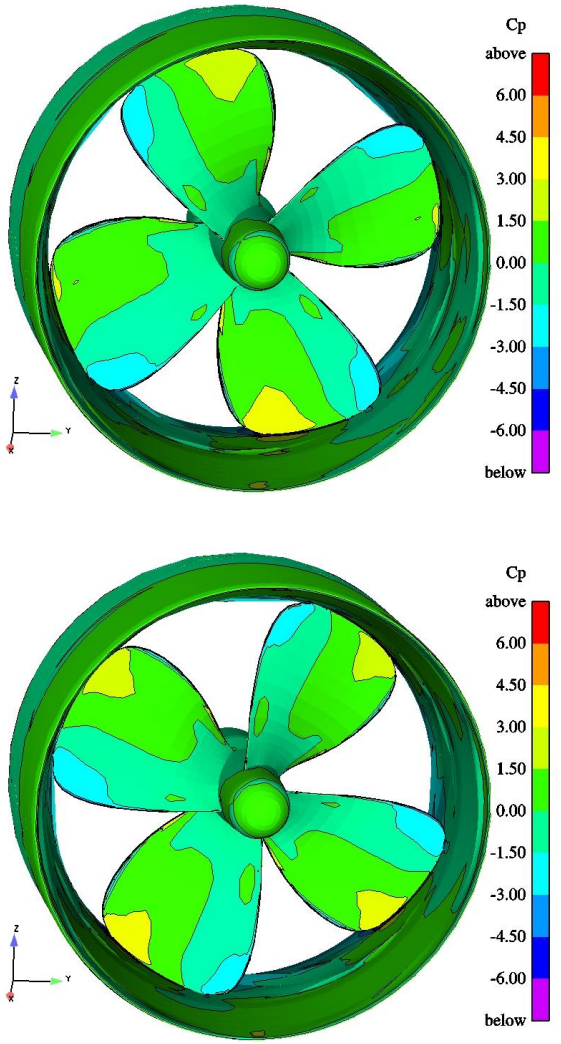

Figure 14. Pressure contours at key blade positions of 22.5 and 67.5 deg. *Time-accurate* computation. Back view without the rudder.

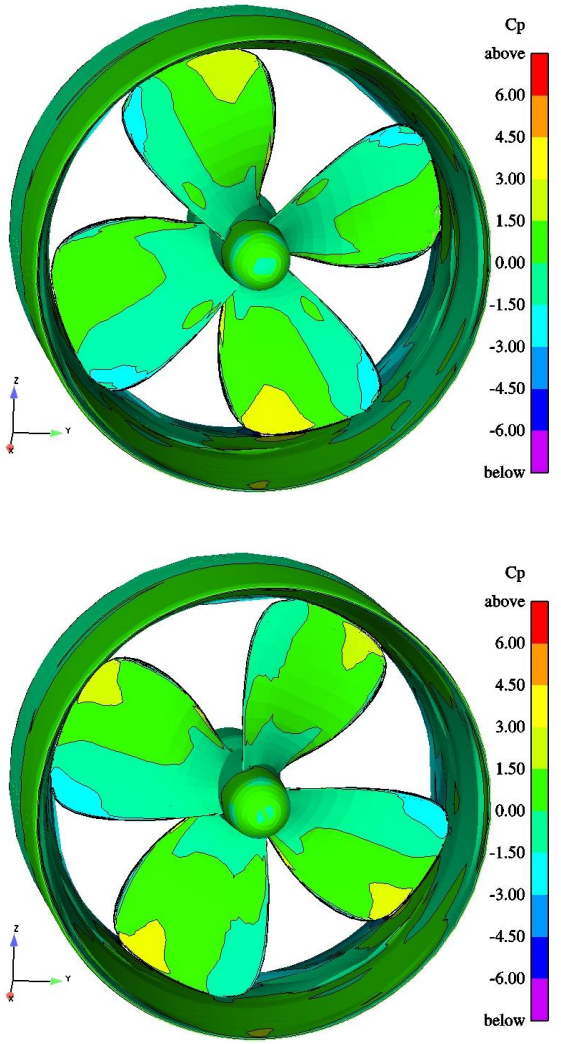

Figure 15. Pressure contours at key blade positions of 22.5 and 67.5 deg. *Quasi-steady* computation. Back view without the rudder.

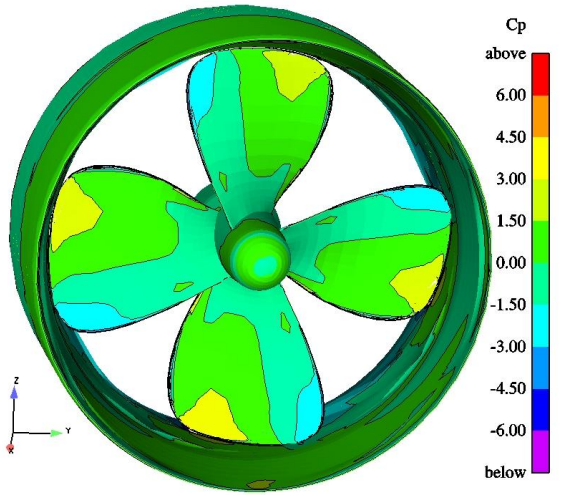

Figure 16. Pressure contours at key blade position of 0 deg. *Mixing plane* computation. Back view without the rudder.

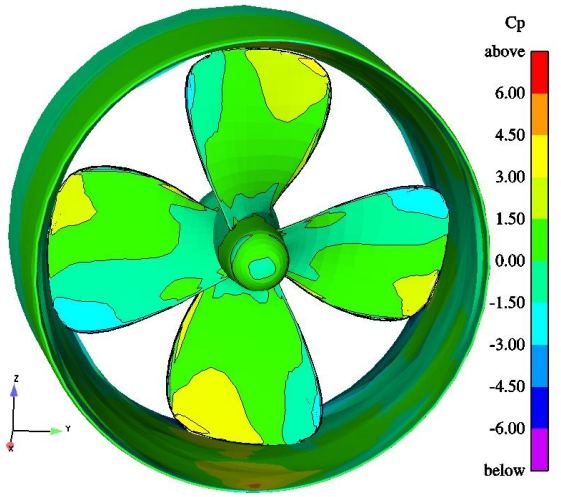

Figure 17. Pressure contours at key blade position of 0 deg. *Quasi-steady* computation *with numerical blockage*. Back view without the rudder.

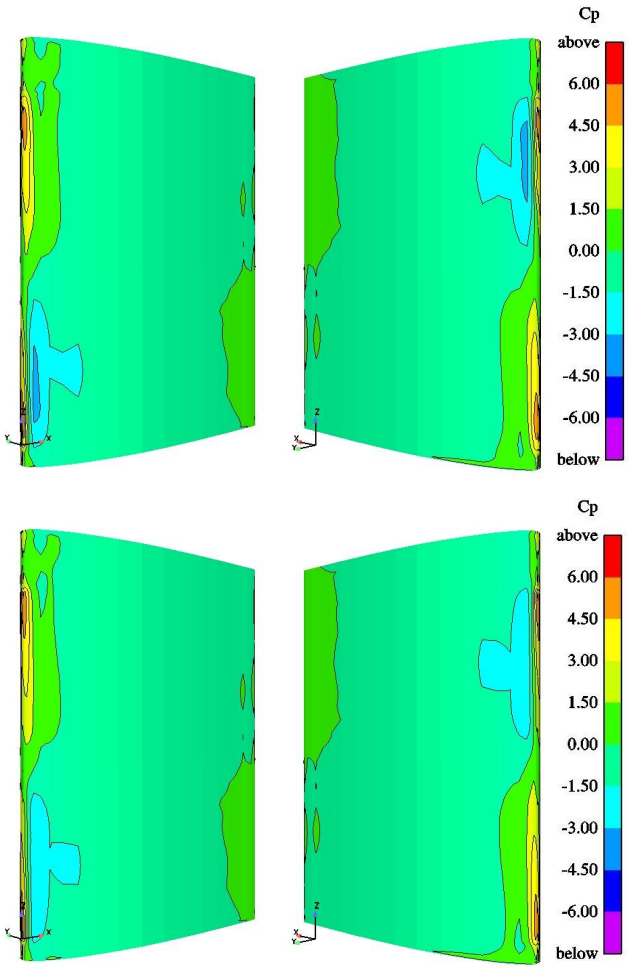

Figure 18. Pressure contours on the rudder at key blade positions of 0 (above) and 45 (below) deg. *Time-accurate* computation.

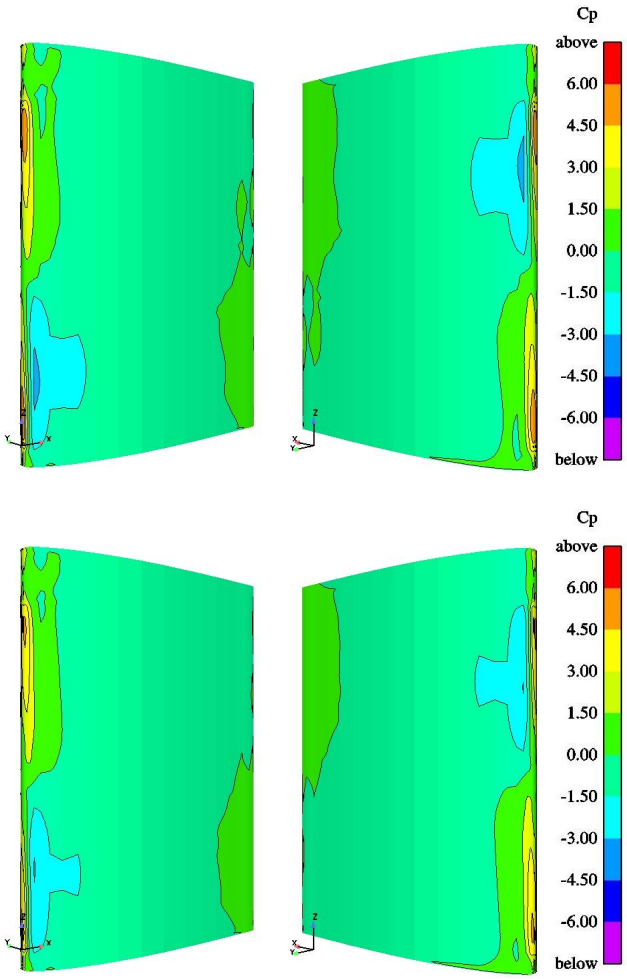

Figure 19. Pressure contours on the rudder at key blade positions of 0 (above) and 45 (below) deg. *Quasi-steady* computation.

between the rotating and stationary domains weak, avoiding in this way numerical flow blockage. This was accomplished by locating the interface between the rotating and stationary blocks far enough upstream in front of the rudder, i.e. midway between the downstream edge of the hub and the blade trailing edge. The other interface upstream the propeller was located in front of the duct. Even though the quasi-steady approach succeeds in yielding representative values of the fluctuation amplitude in thrust on a single blade, it fails in capturing the amplitude of the fluctuation on all blades, which is underpredicted. This was a consequence of the 'too symmetric' time variation of thrust on a single blade resulting from the quasi-steady approach relative to the asymmetric variation resulting from the time-accurate computation.

ACKNOWLEDGEMENTS

This work has been made within the European Union SUPERPROP project. The authors wish to thank the partners in the SUPERPROP consortium. Special thanks are given to PESCANOVA for providing the geometries subject to investigation.

REFERENCES

Li, D.-Q. (2005) "Quasi-steady and unsteady RANS calculations of a highly-skewed propeller in an inclined flow", Proceedings of the 4th IWSH, Shanghai, China.

Sánchez-Caja, A., Rautaheimo, P., Salminen, E., and Siikonen, T. (1999). 'Computation of the Incompressible Viscous Flow around a Tractor Thruster Using a Sliding Mesh Technique'. Proceedings of the 7th International Conference in Numerical Ship Hydrodynamics, Nantes (France).

Sánchez-Caja, A., Rautaheimo, P. and Siikonen, T. (2000). 'Simulation of Incompressible Viscous Flow Around a Ducted Propeller Using a RANS Equation Solver', 23rd Symposium on Naval Hydrodynamics, Val de Reuil (France).

Sánchez-Caja, A. Pylkkänen J.V. and Sipilä, T. P. (2008). 'Simulation of the Incompressible Viscous Flow around Ducted Propellers with Rudders Using a RANSE Solver'. 27th Symposium on Naval Hydrodynamics, Korea